# Green's Functions from Real-Time Bold-Line Monte Carlo Calculations: Spectral Properties of the Nonequilibrium Anderson Impurity Model

Guy Cohen,[1,2] Emanuel Gull,[3] David R. Reichman,[1] and Andrew J. Millis[2]
[1]Department of Chemistry, Columbia University, New York, New York 10027, USA
[2]Department of Physics, Columbia University, New York, New York 10027, USA
[3]Department of Physics, University of Michigan, Ann Arbor, Michigan 48109, USA
(Received 15 October 2013; published 9 April 2014)

The nonequilibrium spectral properties of the Anderson impurity model with a chemical potential bias are investigated within a numerically exact real-time quantum Monte Carlo formalism. The two-time correlation function is computed in a form suitable for nonequilibrium dynamical mean field calculations. Additionally, the evolution of the model's spectral properties are simulated in an alternative representation, defined by a hypothetical but experimentally realizable weakly coupled auxiliary lead. The voltage splitting of the Kondo peak is confirmed and the dynamics of its formation after a coupling or gate quench are studied. This representation is shown to contain additional information about the dot's population dynamics. Further, we show that the voltage-dependent differential conductance gives a reasonable qualitative estimate of the equilibrium spectral function, but significant qualitative differences are found including incorrect trends and spurious temperature dependent effects.

DOI: 10.1103/PhysRevLett.112.146802 PACS numbers: 73.63.Kv, 72.10.Fk, 73.21.La, 85.65.+h

The nonequilibrium physics of strongly correlated systems is a fundamental issue at the cutting edge of research in condensed matter physics. Out-of-equilibrium processes can be manipulated and studied in cold atomic gases [1–3] or by using ultrafast spectroscopy [4,5], and are relevant for the understanding of phenomena ranging from the behavior of atoms [6], molecules [7], and nanocrystals [8] adsorbed on surfaces to transport in molecular electronic devices [9,10]. The problem is theoretically challenging because the strong correlations render perturbative techniques inapplicable while the nonequilibrium aspects preclude the use of most standard statistical-mechanics techniques. The principal methods rely on real-time propagation from some initial condition and are limited in the times which can be accessed. For steady state a numerically exact description in terms of Matsubara voltages can bypass time propagation, but becomes biased by the need to perform analytical continuation [11,12]. Direct equation of motion techniques are sometimes applicable where initial correlations can be neglected [13], but at computational costs similar to direct propagation. The theoretical challenges become particularly acute when one is interested in steady state correlation functions: converged results require propagation to times long enough so that steady state is reached, and beyond that to the times needed to define the correlation function.

One simplifying aspect of many interesting cases is that the important many-body correlations may be taken to be localized in space, either by the physical situation (for example, a quantum dot where the interactions are confined to the region of the dot and the leads may be taken to be noninteracting) or by a theoretical approximation such as dynamical mean field theory (DMFT) which may be formulated both in [14,15] and out of [16,17] equilibrium and provides an approximate solution of the properties of a spatially infinite system in terms of the solution of a quantum impurity model.

A crucial bottleneck in the applications of DMFT to the nonequilibrium situation has been the lack of impurity solvers which can access the long time behavior. In particular, nonequilibrium DMFT requires the evaluation of the dynamical electron propagator, a two-time correlation function. Recent years have seen the development of several controlled nonequilibrium impurity solvers with this capability, including work based on interaction expansion Monte Carlo [18], exact diagonalization [19,20], and hierarchical equation of motion techniques [21–23]. These approaches have provided important insights into the physics of strongly correlated systems out of equilibrium, but all carry intrinsic limitations and are viable only in particular parameter regimes. Monte Carlo methods are restricted by the dynamical sign problem to short propagation times, making it difficult to obtain high-resolution spectral information or access the nonequilibrium steady state [24]. On the other hand, the exact diagonalization and equation of motion methods have a very unfavorable computational scaling because the spectral structure of the noninteracting baths must be represented by a small number of degrees of freedom. A general and unbiased computational scheme capable of representing spectral data at the level required for comparison to experiment or for general DMFT applications remains sorely needed.

Recently, a method for extracting numerically exact spectral information and correlation functions from real-time bold-line

 

[25,26] continuous time Monte Carlo (bold-CTQMC) calculations [27,28] has been put forth [29] which largely circumvents many of the limitations of previous real-time Monte Carlo methods. The method can access substantially longer times than were previously accessible, and in combination with memory function methods [30–32] has been shown to enable the computation of single-time observables, such as the magnetization density, out to unprecedentedly long times [33]. In this Letter we show that the new bold-line methods enable the calculation of the steady-state nonequilibrium two-time electron Green's function and lead to new insights into the evolution of the system towards steady state for the prototypical example of the nonequilibrium Anderson impurity model. We follow the formation of the Kondo peak after a gate quench, showing how the electron spectral function evolves to its steady state value, demonstrate the long-suspected voltage splitting of the Kondo resonance in the presence of a bias voltage [34–40], and establish that the current-voltage characteristic of a quantum dot provides an inaccurate representation of the many-body density of states. The impurity solver described here works in a manner practical for the needs of nonequilibrium DMFT. In particular, the computational complexity of our approach is independent of both the dot-bath coupling density and the final spectral resolution desired.

We have used the bold-line methods [27,28] to directly evaluate two time correlation functions but we find that more accurate and efficient access to the steady-state spectral function may be obtained from a variant of an insightful idea originally proposed as an experimental configuration for probing transport in quantum dots [41,42]. In its original form the idea was to relate the spectral function to the voltage dependence of a current flowing through a single additional weakly coupled auxiliary lead $A$ (Fig. 1, top left):

$$A_{\mathrm{aux}}(V_A,t)=\lim_{\Gamma_A\to 0}-\frac{1}{\Gamma_A\pi}\frac{dI_A(t)}{dV_A}. \tag{1}$$

As $t$ approaches infinity while the auxiliary lead is kept at a fixed chemical potential $V_A$, $A_{\mathrm{aux}}(V_A,t)$ becomes time independent and approaches $A(\omega=V_A)\equiv-(1/\pi)\Im\{G^r(\omega=V_A)\}$. We find [29] that a theoretically more convenient (although experimentally impractical) representation may be achieved by considering the current $I$ flowing between two auxiliary leads (Fig. 1, top right) which are weakly coupled to the systems only at a predefined frequency $\omega'$ [$\Gamma_A=\eta\delta(\omega-\omega')$] with $\eta$ much less than the typical physical coupling $\Gamma$ to the principal leads. We take one of the leads to be full (f: chemical potential much higher than any relevant scale) and one to be empty (e: chemical potential much lower than any relevant scale). Then,

$$A_{\mathrm{aux}}(\omega,t)=\lim_{\eta\to 0}-\frac{2h}{e\pi\eta}[I_A^{\mathrm{f}}(\omega,t)-I_A^{\mathrm{e}}(\omega,t)]. \tag{2}$$

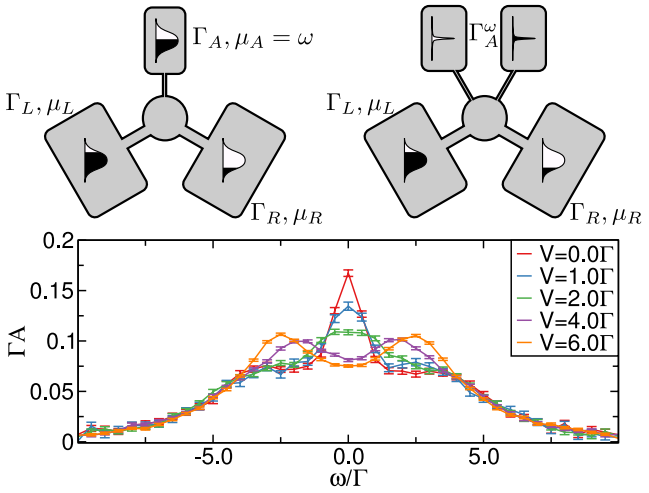


FIG. 1 (color online). The experimental auxiliary lead setup (top left) and the double probe scheme (top right) are illustrated. Below, the steady state spectral function $A(\omega)$ is shown at several voltages. The results are obtained from bold-CTQMC calculations using the double probe auxiliary lead formalism at $\Gamma t=10$. Error bars estimate statistical Monte Carlo errors.

In addition to its computational advantages, this formalism provides physical insight into the evolution of dot properties after a quench. At any given time, the full lead injects electrons into the system at frequency $\omega$ and at a rate of $-I_A^{\mathrm{f}}(\omega,t)$, and should thus (neglecting the response properties of the auxiliary lead itself) be proportional to the density of electronic excitations at this frequency and time; similarly, $I_A^{\mathrm{e}}(\omega,t)$ probes the density of hole excitations. Experimentally, one would only have access to $A_{\mathrm{aux}}$, which is proportional to the total (electron +hole) excitation density. In equilibrium or in steady state outside the bias window (up to $\sim k_BT$) clearly only the empty or full probe contributes and excitations can be distinguished by type. For comparison, if $A(t)$ is obtained only for a finite time interval, its Fourier transform yields only a discrete set of energies approximating $A(\omega)$. Since $A_{\mathrm{aux}}(\omega,t)$ provides frequency-rich information at all times, and since (unlike the two-time correlation function) an experimental pathway for directly measuring it has been suggested, we suggest that it is an interesting and potentially useful quantity to explore in its own right.

The model we treat consists of an Anderson impurity [43] coupled to two leads held at different chemical potentials (upper panels, Fig. 1). Physical realizations include transport in molecular junctions and scanning microscopy studies of adsorbed atoms. However, we emphasize that the method is equally applicable to other nonequilibrium situations including Hamiltonians with explicit time dependence arising in irradiated quantum dots and in the dynamical mean field analysis of pump-probe experiments. Setting $\hbar=e=1$, the Anderson model Hamiltonian is

$$H=H_D+H_B+V, \tag{3}$$

$$H_D = \sum_{\sigma\in\{\uparrow,\downarrow\}} \varepsilon_\sigma d_\sigma^\dagger d_\sigma + U n_\uparrow n_\downarrow, \tag{4}$$

$$H_B = \sum_{a=L,R\sigma k} \varepsilon_{\sigma k} a_{a\sigma k}^\dagger a_{a\sigma k}, \tag{5}$$

$$V = \sum_{a\sigma k} (V_{a\sigma k} a_{a\sigma k}^\dagger d_\sigma + \text{H.c.}). \tag{6}$$

Here, $d_\sigma^\dagger(d_\sigma)$ operators create (destroy) electrons with spin $\sigma = \pm(1/2)$ and energy $\varepsilon_\sigma$ on the dot; $a_{a\sigma k}^\dagger(a_{\sigma k})$ operators create (destroy) electrons with spin $\sigma$ and energy $\varepsilon_{\sigma k}$ in the left ($a = L$) or right ($a = R$) lead, where the indices $k$ enumerate levels; and the $V_{a\sigma k}$ define the dot-lead hybridization (an analogous definition applies to the auxiliary lead). The lead dispersions and the coupling strengths are determined by a coupling density $\Gamma_{L/R}(\omega) = 2\pi\sum_{k\in L/R} V_{\sigma k}^* V_{\sigma k}\delta(\omega - \varepsilon_k)$. In the rest of this Letter we will take the $\Gamma$ to be identical for the two leads and spins (this is done for convenience and is by no means a limitation of the method). We choose a flat, soft-edged coupling density $\Gamma_{L/R}(\omega) = ((\Gamma/2)/(1 + e^{\nu(\omega-\Omega_c)})(1 + e^{-\nu(\omega+\Omega_c)}))$, and in order to keep the discussion simple, all results shown are at an interaction of $U = 6\Gamma$, an inverse temperature of $\beta\Gamma = 3$, a bandwidth of $\Omega_c = 10\Gamma$ and an inverse band edge width of $\nu = 10\Gamma^{-1}$ (except where stated otherwise). The system is expected to have a Kondo temperature of $\sim 0.2\Gamma$. We also hold the chemical potentials in the two leads at a symmetrically applied bias $\mu_{L/R} = \pm(V/2)$ (we note in passing that the main limitation of the method is in accessing low temperatures [27]. Starting from decoupled dot and leads we then time evolve the system for some time $\Gamma t$ until steady state has been reached. The dot is initially empty. The coupling to the auxiliary leads described in the previous chapter is $\eta = 10^{-3}\Gamma$.

The effect of voltage on the spectral function is illustrated in Fig. 1. At zero voltage the Kondo peak can clearly be seen as it begins to form (the temperature studied is at the upper edge of the Kondo regime). With the application of a bias voltage, the peak lowers, widens, and eventually splits. While the magnitude of the Kondo effect decreases when the system is driven away from equilibrium, the effect is obviously not destroyed by the bias, and partial hybridization of the dot with each lead occurs simultaneously. Except at frequencies much higher than the bias, the spectral function is also significantly modified by the nonequilibrium conditions, indicating that the equilibrium spectral function is an inappropriate quantity for the description of nonequilibrium physics. We note that the equilibrium aspects of this problem may be addressed by the numerical renormalization group [44], which is expected to be more efficient at low temperatures. However, outside equilibrium this has never been achieved, and it has been suggested that this is due to a fundamental limitation of the Wilson mapping [45].

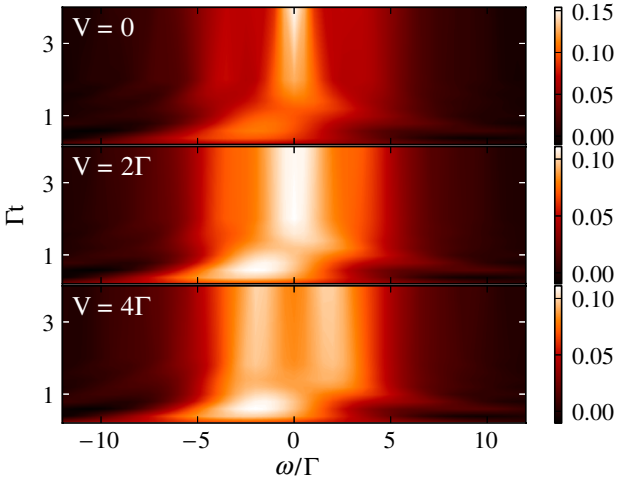


FIG. 2 (color online). The time evolution of the spectral function $A_{\text{aux}}(\omega)$ shown at several voltages, obtained from bold-CTQMC calculations using the double-probe auxiliary lead formalism, with $\eta = 10^{-3}\Gamma$.

The time dependence of $A_{\text{aux}}$ is illustrated in Fig. 2, which shows what the results of a time-dependent measurement of $A_{\text{aux}}$ would look like if the dot begins devoid of electrons and decoupled from all leads. At short times, near the bottom edge of each of the three panels, a peak forms (before disappearing) near the single-particle resonance energy $\varepsilon_\sigma = -3\Gamma$. This corresponds to the availability of electronic levels and is quickly followed by the formation of corresponding hole levels at positive frequencies, though experimentally we would not be able to distinguish electrons from holes. At longer times, as the dot begins to fill, one can observe near the top edges of the panels the formation of the steady-state spectral properties including the equilibrium Kondo resonance (top panel) and its voltage widened (middle panel) and split (bottom panel) variations. The calculated quantity (and the hypothetical experiment) therefore provides direct access not only about steady-state spectral properties, but also to the dynamical evolution of the system's total density of single particle excitations. Combined with knowledge about the initial conditions, this provides information about the population dynamics.

A more conventional view of the dynamics is provided in Fig. 3. Here we display the standard spectral function $A(\omega)$ at $V = 0$ and $V = 4\Gamma$ as a two-time correlation function (left panels) and as a function of frequency and time (right panels). Notably, these correlation functions are exactly the objects used in time-dependent DMFT [18,46]. The frequency-space property is obtained from the discrete Fourier transform of the two-time property. The two-time correlations exhibit little structure in the cases shown, due to the lack of explicit time dependence in the Hamiltonian, but interestingly the nonequilibrium nature of the dynamical evolution actually adds some noticeable correlations at long times. At finite times frequency resolution is limited to

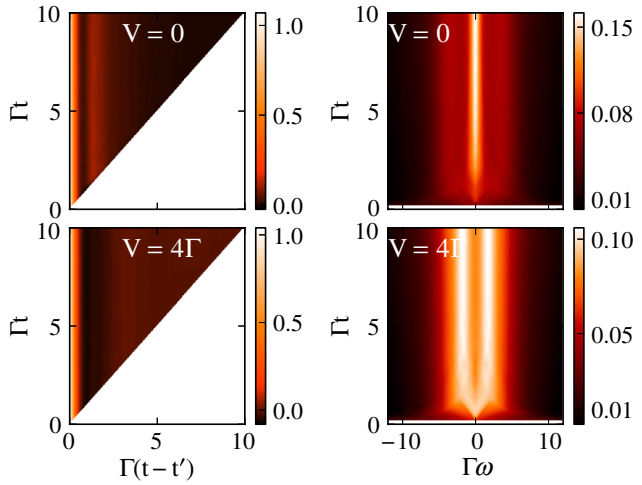


FIG. 3 (color online). The time evolution of the real part of the retarded Green's function $\Re\{G^r(t,t-t')\}$ (left panels) and the spectral function $A(\omega)$ (right panels) at voltages indicated, as calculated from two time correlation functions within bold-CTQMC calculations.

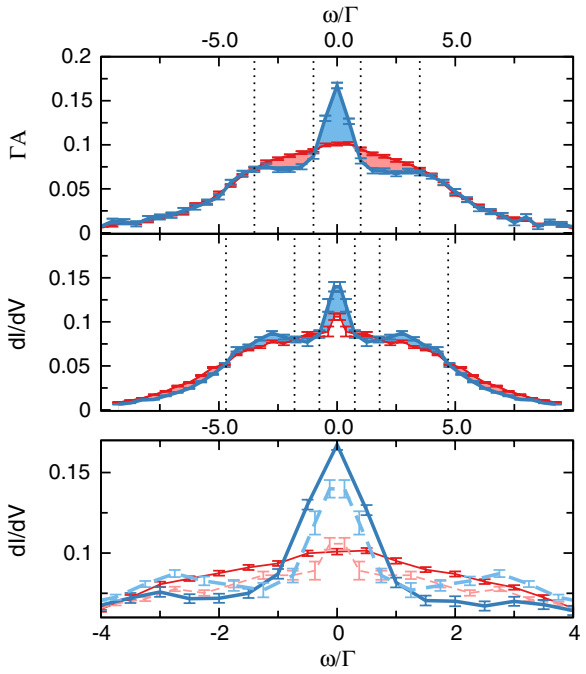


FIG. 4 (color online). The steady state spectral function $A(\omega)$ (upper panel) compared to the steady state differential conductance (middle panel) as a function of half the voltage at two different inverse temperatures $\beta$. Both observables are obtained from bold-CTQMC at $\Gamma t = 10$. The area between the curves are shaded according to the maximal value and vertical dotted lines mark crossing points. The bottom panel displays all results: the solid lines are the spectral function and the dashed curves are the differential conductance.

$\Delta\omega = (\pi/t)$, where $t$ is the propagation time. In the finite voltage case, it actually seems as if a central peak forms before the peak splitting occurs, which differs from what is observed when $A_{\text{aux}}$ is examined. Also, unlike $A_{\text{aux}}$, $A$ obeys particle-hole symmetry at all times.

Within linear deviations from equilibrium in the voltage, the normal differential conductance through the device—that is, the voltage derivative of the current $I$ through the strongly coupled left or right terminal—can be interpreted as an estimator for the equilibrium spectral function. However, as Fig. 1 clearly shows, the application of voltage beyond the linear response regime significantly modifies the spectral density. It is therefore of some interest to see how the use of normal current in the nonequilibrium case fares in practice as a measure of equilibrium properties within a numerically exact framework. The top panel of Fig. 4 shows the equilibrium spectral function at two different inverse temperatures. Below this, the lower panel of Fig. 4 displays the steady state differential conductance for the same parameter sets.

The two heavy blue $\beta\Gamma = 3$ curves or the two lighter red $\beta\Gamma = 1$ curves appear superficially similar at first glance. The clearest differences are a slight lowering and narrowing of the Kondo peak, a slight accentuation of the Hubbard peaks, and a small Kondo-like peak which appears in the differential conductance at a temperature where it does not yet exist in the spectral function. Comparing the two sets of curves side by side, however, brings the inaccuracies of the differential conductance as an estimator for the spectral function into sharp contrast: the differential conductance exhibits a high-frequency temperature dependence completely absent from the spectral function, with a temperature dependent trend at intermediate frequencies that is actually reversed. A certain degree of caution is therefore appropriate when applying the linear-response interpretation to current measurements.

To summarize, we have implemented the computation of Green's functions within real time bold-QMC calculations in nonequilibrium using both correlation functions and a double-probe auxiliary current formalism. We obtained the spectral function of the nonequilibrium Anderson model and demonstrated the voltage splitting of the Kondo peak within a general, numerically exact framework. Through our formalism the dynamics of the excitation density of states starting with a coupling or gate quench and up to the formation of a Kondo peak was studied, with and without a bias voltage (the formalism is also applicable to other quench types, such as voltage, temperature, or interaction quenches). We have shown that the auxiliary lead interpretation and the associated experimental setup provides access not only to steady state spectral properties, but also to information about the excitation and (indirectly) population dynamics of the system. Finally, we have discussed the use of current measurements in the more common two lead setup to access the equilibrium spectral properties of the Anderson model, demonstrating that while the differential conductance provides a good qualitative estimator for spectral functions, it also fails in reproducing temperature trends at lower frequencies while introducing spurious trends at high ones.

Looking forward, the tools presented here not only provide new insight into transport in quantum impurity models, but also provide the functionality required by an impurity solver within nonequilibrium DMFT: bold-CTQMC calculations can provide spectral data which can be incorporated into DMFT calculations incorporating multiple leads at different thermodynamic parameters, as well as two time correlation functions for time-dependent DMFT. It is practically useful up to times and interaction strengths substantially greater than those of previous Monte Carlo methods, while maintaining the critical advantage of the Monte Carlo method in resolution over other methods. The bold-CTQMC method is therefore expected to have important consequences in the study of strongly correlated systems out of equilibrium.

The authors would like to thank Rainer Härtle and Eran Rabani for their many insightful comments. G. C. is grateful to the Yad Hanadiv-Rothschild Foundation for the award of a Rothschild Postdoctoral Fellowship and NSF DMR 1006282. G. C. and E. G. acknowledge TG-DMR120085 and TG-DMR130036 for computer time. D. R. R. acknowledges NSF CHE-1213247. A. J. M. acknowledges NSF DMR 1006282. E. G. acknowledges DOE ER 46932. Our implementations were based on the ALPS [47] libraries.

[1] O. Mandel, M. Greiner, A. Widera, T. Rom, T. W. Hänsch, and I. Bloch, Phys. Rev. Lett. **91**, 010407 (2003).
[2] T. Kinoshita, T. Wenger, and D. S. Weiss, Nature (London) **440**, 900 (2006).
[3] S. Hofferberth, I. Lesanovsky, B. Fischer, T. Schumm, and J. Schmiedmayer, Nature (London) **449**, 324 (2007).
[4] S. Iwai, M. Ono, A. Maeda, H. Matsuzaki, H. Kishida, H. Okamoto, and Y. Tokura, Phys. Rev. Lett. **91**, 057401 (2003).
[5] L. Perfetti, P. A. Loukakos, M. Lisowski, U. Bovensiepen, H. Berger, S. Biermann, P. S. Cornaglia, A. Georges, and M. Wolf, Phys. Rev. Lett. **97**, 067402 (2006).
[6] V. Madhavan, W. Chen, T. Jamneala, M. F. Crommie, and N. S. Wingreen, Science **280**, 567 (1998).
[7] A. Zhao, Q. Li, L. Chen, H. Xiang, W. Wang, S. Pan, B. Wang, X. Xiao, J. Yang, J. G. Hou, and Q. Zhu, Science **309**, 1542 (2005).
[8] D. Mocatta, G. Cohen, J. Schattner, O. Millo, E. Rabani, and U. Banin, Science **332**, 77 (2011).
[9] J. Park, A. N. Pasupathy, J. I. Goldsmith, C. Chang, Y. Yaish, J. R. Petta, M. Rinkoski, J. P. Sethna, H. D. Abruna, P. L. McEuen, and D. C. Ralph, Nature (London) **417**, 722 (2002).
[10] J. R. Heath and M. A. Ratner, Phys. Today **56**, 43 (2003).
[11] J. E. Han and R. J. Heary, Phys. Rev. Lett. **99**, 236808 (2007).
[12] A. Dirks, P. Werner, M. Jarrell, and T. Pruschke, Phys. Rev. E **82**, 026701 (2010).
[13] J. Jin, X. Zheng, and Y. J. Yan, J. Chem. Phys. **128**, 234703 (2008).
[14] A. Georges, G. Kotliar, W. Krauth, and M. J. Rozenberg, Rev. Mod. Phys. **68**, 13 (1996).
[15] A. Georges, AIP Conf. Proc. **715**, 3 (2004).
[16] J. K. Freericks, V. M. Turkowski, and V. Zlatić, Phys. Rev. Lett. **97**, 266408 (2006).
[17] J. K. Freericks and V. M. Turkowski, J. Phys. Conf. Ser. **35**, 39 (2006).
[18] M. Eckstein, M. Kollar, and P. Werner, Phys. Rev. Lett. **103**, 056403 (2009).
[19] E. Arrigoni, M. Knap, and W. von der Linden, Phys. Rev. Lett. **110**, 086403 (2013).
[20] C. Gramsch, K. Balzer, M. Eckstein, and M. Kollar, Phys. Rev. B **88**, 235106 (2013).
[21] Z. H. Li, N. H. Tong, X. Zheng, D. Hou, J. H. Wei, J. Hu, and Y. J. Yan, Phys. Rev. Lett. **109**, 266403 (2012).
[22] S. Wang, X. Zheng, J. Jin, and Y. Yan, Phys. Rev. B **88**, 035129 (2013).
[23] D. Hou, R. Wang, N. Tong, J. Wei, X. Zheng, and Y. Yan (to be published).
[24] A. Dirks, M. Eckstein, T. Pruschke, and P. Werner, Phys. Rev. E **87**, 023305 (2013).
[25] N. Prokof'ev and B. Svistunov, Phys. Rev. Lett. **99**, 250201 (2007).
[26] N. V. Prokof'ev and B. V. Svistunov, Phys. Rev. B **77**, 125101 (2008).
[27] E. Gull, D. R. Reichman, and A. J. Millis, Phys. Rev. B **82**, 075109 (2010).
[28] E. Gull, D. R. Reichman, and A. J. Millis, Phys. Rev. B **84**, 085134 (2011).
[29] G. Cohen, D. R. Reichman, A. J. Millis, and E. Gull, Phys. Rev. B **89**, 115139 (2014).
[30] G. Cohen and E. Rabani, Phys. Rev. B **84**, 075150 (2011).
[31] G. Cohen, E. Y. Wilner, and E. Rabani, New J. Phys. **15**, 073018 (2013).
[32] E. Y. Wilner, H. Wang, G. Cohen, M. Thoss, and E. Rabani, Phys. Rev. B **88**, 045137 (2013).
[33] G. Cohen, E. Gull, D. R. Reichman, A. J. Millis, and E. Rabani, Phys. Rev. B **87**, 195108 (2013).
[34] Y. Meir, N. S. Wingreen, and P. A. Lee, Phys. Rev. Lett. **70**, 2601 (1993).
[35] S. De Franceschi, R. Hanson, W. G. van der Wiel, J. M. Elzerman, J. J. Wijpkema, T. Fujisawa, S. Tarucha, and L. P. Kouwenhoven, Phys. Rev. Lett. **89**, 156801 (2002).
[36] R. Leturcq, L. Schmid, K. Ensslin, Y. Meir, D. C. Driscoll, and A. C. Gossard, Phys. Rev. Lett. **95**, 126603 (2005).
[37] R. Leturcq, L. Schmid, K. Ensslin, D. C. Driscoll, and A. C. Gossard, Phys. Status Solidi B **243**, 3653 (2006).
[38] N. Shah and A. Rosch, Phys. Rev. B **73**, 081309 (2006).
[39] P. Fritsch and S. Kehrein, Phys. Rev. B **81**, 035113 (2010).
[40] M. Pletyukhov and H. Schoeller, Phys. Rev. Lett. **108**, 260601 (2012).
[41] E. Lebanon and A. Schiller, Phys. Rev. B **65**, 035308 (2001).
[42] Q.-f. Sun and H. Guo, Phys. Rev. B **64**, 153306 (2001).
[43] P. W. Anderson, Phys. Rev. **124**, 41 (1961).
[44] T. A. Costi, A. C. Hewson, and V. Zlatic, J. Phys. Condens. Matter **6**, 2519 (1994).
[45] A. Rosch, Eur. Phys. J. B **85**, 1 (2012).
[46] M. Eckstein and P. Werner, Phys. Rev. B **82**, 115115 (2010).
[47] B. Bauer*et al.*, J. Stat. Mech. (2011) P05001.